

Article

Influences of Liquid Viscosity and Relative Velocity on the Head-On Collisions of Immiscible Drops

Jiaqing Chang , Rongchang Xu, Jinsheng Cui, Qiaolin Song and Teng Shen * 

School of Mechanical and Electrical Engineering, Guangzhou University, Guangzhou 510006, China

* Correspondence: shent215@gzhu.edu.cn

Abstract: Many researchers have devoted themselves to the collision processes of binary droplets of the same liquid. However, the liquids used in their study were limited, and the phase diagram of the collision outcome was depicted in terms of the Weber and the non-dimensional impact parameter. In this research, the variety of liquid was broadened, and the phase diagram characterized by the Weber number and the Ohnesorge number for head-on collisions of immiscible drops was provided. First, a ternary flow model of binary collision of immiscible drops in quiescent ambient air was proposed. Second, the three-phase fluid interface was tracked and updated by iterating the VOF (Volume of Fluid) functions. The flow field was also updated with the PISO (Pressure-Implicit with Splitting of Operators) algorithm. Finally, the effects of the impact velocity and the viscosities of the liquids on the deformation degree of droplets were analyzed.

Keywords: droplet collision; immiscible drops; encapsulation; droplet deformation



Citation: Chang, J.; Xu, R.; Cui, J.; Song, Q.; Shen, T. Influences of Liquid Viscosity and Relative Velocity on the Head-On Collisions of Immiscible Drops. *Energies* **2022**, *15*, 8544. <https://doi.org/10.3390/en15228544>

Academic Editors: Xinyu Wang, Jingzhi Zhang and Gongming Xin

Received: 16 September 2022

Accepted: 12 November 2022

Published: 15 November 2022

Publisher's Note: MDPI stays neutral with regard to jurisdictional claims in published maps and institutional affiliations.



Copyright: © 2022 by the authors. Licensee MDPI, Basel, Switzerland. This article is an open access article distributed under the terms and conditions of the Creative Commons Attribution (CC BY) license (<https://creativecommons.org/licenses/by/4.0/>).

1. Introduction

The study of droplet collisions first attracted the attention of meteorologists, aiming at understanding the rules of the evolution of clouds [1–5]. Later, with the development of spray combustion and microfluidic technologies, more and more researchers began to pay attention to the droplet collision phenomenon [6–9]. Most researchers studied the stability and sizes distribution of droplet collisions. In particular, the collision regimes were classified, and the phase diagram of the collision outcome was drawn in their works [10–15]. Unfortunately, the studies on the distribution and variation of flow fields were sparse because the droplet velocity is easily affected by the aerodynamic force of the host medium (ambient air, for example).

The process of droplet collision is so complicated that a theoretical description by analytical means is not practical. Typically, experimental observations have provided insights into the regularities of this phenomenon. When two droplets collide in the air or another medium, the outcome of the collision falls into the following categories: permanent coalescence, bouncing, and temporary coalescence followed by reflexive or stretching separation [16–24]. However, the stretching separation mode is unlikely to happen for head-on droplet collision. The impact parameter and the Weber number are usually used to characterize the collision regimes.

The collision between immiscible droplets can be regarded as a three-phase problem [25–28]. Presence of the third fluid makes the modeling of the collision process even more complicated. First, it not only adds two more interfaces to the problem, but also increases the number of parameters (interfacial tension, density, or viscosity). Additionally, the added interface should be tracked with some extra functions; the parameters or state variables across the interfaces may have jump characteristics and should be dealt with.

Compared with the experimental studies, the simulation of the droplet collision has some benefits, such as the intuitive display of the temporal and spatial evolutions of the surfaces of the droplets, the quick variation of the physical parameters of the fluids or

the collision parameters, and the conveniences and low costs. To track the interfaces, the most used methods are the volume-of-fluids (VOF) or level-set methods [29–33]. Besides the simulation of the droplet collisions by the continuum mechanics method, the lattice-Boltzmann method [34–37] and the smoothed-particle hydrodynamics method [38–40] were also usually used in recent years. The studies on the collision processes of binary droplets of different liquids are summarized in Table 1. It can be found that the research on the collision process of immiscible droplets is sparse, especially the modeling study.

Table 1. Summary of the studies of the collisions between two droplets of different liquids.

Authors	Modeling or Experimental Study	Miscible or Immiscible	Droplet Size or Size Ratio	Equal or Different Properties	Ambient Medium	Dimensionless Numbers or Relative Velocity [m/s]
Focke et al. [25]	Modeling and experiment	Miscible	380–750 μm ; Ratio = 0.66, 1.0.	Only different viscosity	Air	$U_{\text{rel}} = 1.0\text{--}3.0$; $15 < We < 133$ (app.)
Choi et al. [26]	Modeling	Immiscible	40 μm (equal-sized)	Only different surface tension	Liquid	$Re = 0.25$
Nishio et al. [40]	Modeling	Immiscible	~ 200 μm	All different	Air	$U_{\text{rel}} = 2.0, 3.0, 3.2$
Zhang et al. [27]	Modeling	Immiscible	Equal-sized	Only different surface tension	Air	$3 < We < 600$
Ebadi et al. [37]	Modeling	Immiscible	50–200 μm (app.)	All different	Liquid	$We > 40$ & $Ca > 1$ & $0.2 < Oh < 0.3$
Gao et al. [41]	Experiment	Miscible	400–600 μm (equal-sized)	All different	Air	$10 < We < 100$
Chen et al. [42,43]	Experiment	Immiscible	700–800 μm (equal-sized)	All different	Air	$0 < We < 100$ & $30 < Re < 500$
Roisman et al. [18]	Experiment	Immiscible	180–210 μm (equal-sized)	All different	Air	$U_{\text{rel}} = 2.0\text{--}7.0$ (app.)
Planchette et al. [13,17,21]	Experiment	Immiscible	150–350 μm (equal-size)	All different	Air	$50 < Re < 400$ & $0.02 < Oh < 0.5$ (app.)
Zhang et al. [44]	Experiment	Immiscible	~ 160 μm (equal-sized)	All different	Silicone oil	Not provided
Piskunov et al. [45]	Experiment	Both	0.2–10 mm (equal-sized)	All different	Air	$U_{\text{rel}} = 0.5\text{--}10.0$ (app.)

In this paper, the head-on collision processes of immiscible droplets were systematically simulated. First, a computation model, which considered the three fluid phases and their interfacial tensions was proposed. The governing equations were the transport equation and the Navier–Stokes equations, which regulated the dynamics of the liquids and the topological changes in the interfaces between the air phase, the oil phase, and the aqueous phase. The positions and shapes of these interfaces were tracked so that the surface tension forces can be derived from the curvature of the interfaces. Second, a mesh dependency study was conducted and the simulation results were compared with the result of a previous experiment. Third, the influence of the collision velocities and the fluid viscosities (including the encapsulated phase and the encapsulating phase) on the collision results were analyzed. Last, the phase diagram of the collision outcome, which was usually depicted in terms of the non-dimensional impact parameter and the Weber number, was characterized by the Weber and Ohnesorge number in this study on the consideration that the various liquids used.

The featured work of this paper is reflected in the following three aspects: (1) The fluids used in this paper were different and immiscible, and the ranges of the physical parameters were wide. (2) The deformation of the liquid disk, which formed after the collision contact, was found closely related to the viscosity difference between the colliding droplets. (3) The phase diagram of the outcome of droplet collision was depicted in terms of the Weber and Ohnesorge numbers, which shows the influence of the physical parameters on the collision outcome more intuitively.

2. Model and Numerical Algorithm

In this research, the shape evolution process of the droplet after collision contact in an air medium was studied. This problem can be considered as a two-dimensional problem

because it is axisymmetric regardless of the geometry or the boundary conditions. Since the droplets are immiscible and cannot penetrate each other, the VOF method was used to track the free surface during the droplet collision process. In the VOF method, a variable (α) is used to represent the phase function, which means the volume fraction of a fluid in a grid cell. The phase interface of each cell can be tracked by the volume fraction function (α).

For a particular grid, its volume fraction function can be one of the following three cases.

- (a) $\alpha_p = 0$: there is no P-phase fluid in the current grid;
- (b) $\alpha_p = 1$: the current grid is wholly occupied by the P-phase fluid;
- (c) $0 < \alpha_p < 1$: the current grid has a boundary between the P-phase fluid and one or both of the other phases.

2.1. Governing Equations

In the VOF method, different fluid components share the same set of momentum equations. Generally, the fluid phase with the lowest density is regarded as the primary phase, and the rest of the fluid is regarded as the secondary phase. Therefore, in this study, the air was considered as the primary phase and the liquids as the secondary phase.

The trace of the fluid interface was obtained by solving the transport equation of the liquid phases:

$$\frac{\partial \alpha_q}{\partial t} + \nabla \cdot (\alpha_q \vec{v}) = 0, \quad q = L1, L2. \quad (1)$$

The volume distribution function of the air phase was calculated by the following constraints:

$$\alpha_G + \alpha_{L1} + \alpha_{L2} = 1. \quad (2)$$

The momentum conservation equation along the three coordinate axes (x, y, z) was:

$$\frac{\partial}{\partial t} (\rho_m \vec{v}) + \nabla \cdot (\rho_m \vec{v} \vec{v}) = -\nabla P + \nabla \cdot [\mu_m (\nabla \vec{v} + \nabla \vec{v}^T)] + \vec{F}, \quad (3)$$

where ρ_m and μ_m were the volumetric average density and the volumetric average viscosity of a computation unit, respectively. The physical parameters of each grid cell were shared by each phase and can be calculated by the equations shown below.

$$\rho_m = \alpha_G \rho_G + \alpha_{L1} \rho_{L1} + \alpha_{L2} \rho_{L2} \quad (4)$$

$$\mu_m = \alpha_G \mu_G + \alpha_{L1} \mu_{L1} + \alpha_{L2} \mu_{L2} \quad (5)$$

In the momentum conservation equation, \vec{F} was the momentum source term, which was mainly used to consider the influence of gravity and surface tension. The gravity term can be obtained by including the volume force ($\rho \vec{g}$) directly in the momentum equation. However, the surface tension term required the continuous surface model (CSF) to transform the surface tension into an equivalent volume force (\vec{F}_σ). For a grid cell, the surface tension source term (\vec{F}_σ) can be calculated as:

$$\vec{F}_{\sigma pq} = \sum_{\text{pairs } pq, p < q} \sigma_{pq} \frac{\alpha_p \rho_p \kappa_q \nabla \alpha_q + \alpha_q \rho_q \kappa_p \nabla \alpha_p}{\frac{1}{2}(\rho_p + \rho_q)} \quad p, q = G, L1, L2 \quad (6)$$

where ∇ was the gradient operator, and κ_p and κ_q were the local curvature of the two phases.

For the convenience of discussion, the formulas of the Weber number and the Ohnesorge number were given below.

$$We = \frac{\rho_q D_0 U_r^2}{\sigma_q}, \quad (7)$$

$$Oh = \frac{\mu_q}{\sqrt{\rho_q D_0 \sigma_q}}, \quad (8)$$

where U_r was the initial relative velocity between the colliding droplets; D_0 was the primary diameter of the equal-sized droplets at the initial time; ρ_q , σ_q , and μ_q were the density, surface tension, and dynamic viscosity of the aqueous phase, respectively. For the collision of immiscible droplets, the Weber number and the Ohnesorge number were defined using the physical parameters of the aqueous phase.

2.2. Model and Boundary Conditions

Mohammadi et al. [32] showed that when the size of the continuous phase region is greater than 5 times the diameter of the equal-sized collision droplets, increasing the size of the continuous phase region further in the simulation does not affect the results. As shown in Figure 1a, the simulation area had a square shape in this study. To ensure that all the droplet deformations occurred within the simulation region, the continuous phase region was specified as 10 times the droplet diameter. The two colliding droplets had the same diameter $D_0 = 200 \mu\text{m}$, and the whole calculation area was $2 \times 2 \text{ mm}$ in all simulation cases. The upper and lower boundaries of the continuous phase were set as the wall surfaces, and the front and rear boundaries were set as the pressure outlets. The ambient gas was the atmosphere under normal pressure. The local grids containing two droplets at the initial time are shown in Figure 1b. The initial distance between the two droplets is $0.5 D_0$, and the refined meshes were used to distinguish the droplet or the tiny structures that may be generated during the collision process, such as the small gas film between the drops when they approach each other.

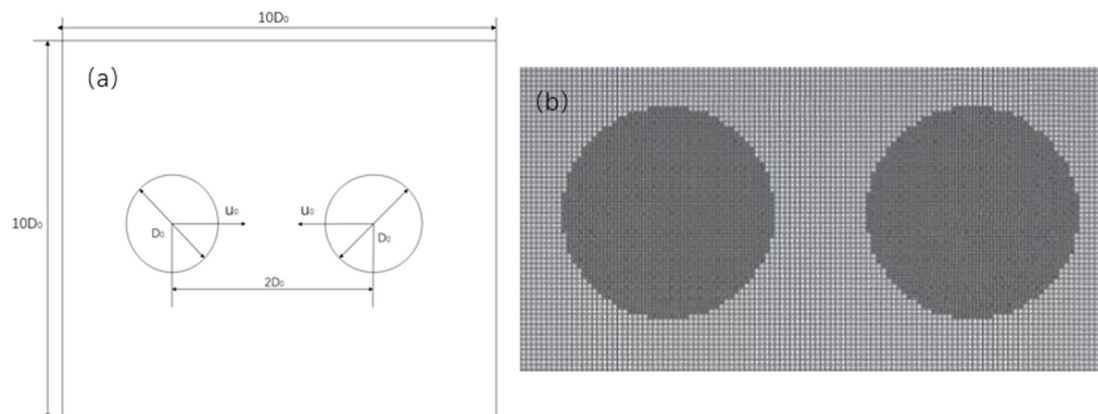


Figure 1. Computational domain (a) and the local grids containing the two droplets at the initial time (b).

2.3. Simulation Strategies

The volume fractions were updated through an explicit interpolation scheme which is shown below.

$$\frac{\alpha_q^{n+1} \rho_q^{n+1} - \alpha_q^n \rho_q^n}{\nabla t} V + \sum_f (\rho_q U_q^n \alpha_q^n) = 0, \quad q = L1, L2, \quad (9)$$

where the superscripts “ $n + 1$ ” and “ n ” meant the variable value at the current time step and the previous time step, respectively, ∇t was the time step size, α_q was the volume fraction of the aqueous phase or the oil phase, U_q was the volume flux through the cell face, V was the volume of cell, and f was the face number.

The droplet collision process was simulated by the Fluent software, which used the cell register to store and update the information of cells, such as volume fraction, density, and so on. Moreover, the DAT (Dynamic Adaption Technique) enabled the Fluent software to adapt the mesh while the calculation was proceeding automatically. The PRESTO (Pressure staggering option) scheme, which was robust for all meshes and had a second-order accuracy, was used for the pressure interpolation. The second-order accurate upwind

scheme was used to discretize the spatial difference in the momentum equation. The PISO scheme, which had a higher degree of accuracy for the approximate relation between the pressure and velocity, was used to decouple the pressure-velocity fields.

In this work, the typical colliding velocity of droplets was 2.0 m/s, and the time step was set as 2×10^{-7} s, so the moving distance of a droplet in a single time step was 4×10^{-7} m. Considering that the minimum grid size was 2.5×10^{-6} m, the time step selected was appropriate because the droplet needs 6.25 time steps to move a grid distance.

2.4. Mesh Independence

A mesh dependence study was conducted to analyze the influence of mesh density on the simulation results. The computed collision processes between a water droplet and a diesel oil droplet are shown in Figure 2a–c under different mesh densities. The relative colliding velocities were all the same at 2.4 m/s. The coarse, moderate, and refined meshes had a minimum cell size of 3.0, 2.5, and 2.0 μm , corresponding to the cell numbers of 176,889, 256,000, and 410,004, respectively. The results showed that it was difficult to find any inconsistency between the computation results of the moderate mesh and refined mesh. However, the computation time for the refined mesh was up to 25 h on a computer with a core frequency of 3.6 GHz. To save time, the moderate mesh was adopted for the simulation cases in the rest of the paper.



Figure 2. Computed droplet collision processes of the model under the same conditions except for the mesh density: (a) coarse mesh, (b) moderate mesh, and (c) refined mesh.

3. Simulation Results

3.1. Comparison with Experiments

We compared the simulation results with the previous experimental results [13] of the droplet collision process between a droplet of a water/glycerol mixture (aqueous phase) and a silicone oil droplet (oil phase) under the same conditions. Both droplets are 200 μm in diameter. The density and viscosity of the water/glycerol droplet (G50, 50% water and 50% glycerol in volume fraction) were 1126.0 kg/m^3 and 6.0 $\text{mPa}\cdot\text{s}$, respectively. The surface tension between the aqueous droplet and air was 68.6 mN/m . The density and viscosity of the silicone oil (SO M2) were 951.8 kg/m^3 and 19.0 $\text{mPa}\cdot\text{s}$, and the surface tension between the oil droplet and air was 20.7 mN/m . The interfacial tension between the two droplets was 36.0 mN/m . The relative velocity of the two droplets was 3.88 m/s, and the collision non-dimensional parameters were $\text{Re} = 145.6$ and $\text{We} = 49.4$. In Figure 3, the black droplet is the aqueous phase (G50), and the gray droplet is the oil phase (SO M2). When the oil droplet and the aqueous droplet collided head-on at the same speed, the aqueous droplet appeared more “solid” because the surface tension of the aqueous drop was greater than that of the oil drop. The oil droplet spread along the surface of the aqueous droplet to form a composite droplet. If the collision speed was moderate, the oil droplet

appeared to “engulf” the aqueous droplet and had the opportunity to encapsulate it, which was the case shown in Figure 3. If the collision speed became greater, the oil droplet and aqueous droplet would expand along the radial direction after the contact and then form a relatively large composite liquid disk, which will eventually split into several small composite droplets. The determinant of the split or coalescence of the composite disk was the competition effect between energies. The simulation results were almost consistent with the experimental results, which verifies the correctness of the simulation algorithm. The comparison shows that the constructed model can be used to study the head-on collision of Newtonian droplets.

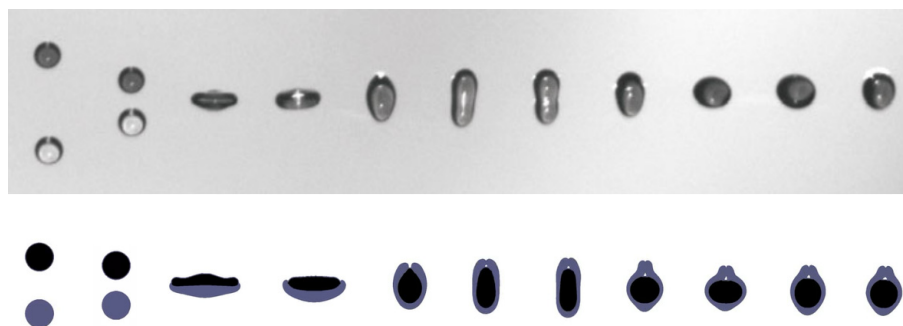


Figure 3. Snapshots and simulation images of the head-on collision process of immiscible droplets.

3.2. Effects of the Weber Number

As shown in Figure 4, we simulated the head-on collision process between a water droplet and a diesel droplet in an air medium with different Weber numbers. Table 2 lists the physical properties of the diesel and the water.

As shown in Figure 4a, the two droplets collided head-on, deformed slightly, and finally coalesced under the action of the interfacial tension (not completely wrapped). The collision results shown in Figure 4b are very similar. The two droplets contacted at 0.1 ms and reached the maximum radial and axial deformation at 0.57 ms and 1.1 ms, respectively. When the collision speed was increased appropriately, as shown in Figure 4c,d, the two droplets coalesced and became fully wrapped. The radial deformation reached a maximum at 0.48 ms, and 0.38 ms, respectively, at which point the kinetic energy was the minimum and the surface energy was the maximum. After that, the droplets began to shrink under the action of the surface force and viscous force, and the liquid of the circumferential edge returned to the middle, which means that the surface energy was gradually converted into kinetic energy. In general, due to the relatively low velocity of the droplets, the kinetic energy was not enough to overcome the joint binding of the viscous force and the surface force. After several axial and radial deformation transitions, the composite droplet finally became wholly wrapped.

As shown in Figure 4e, if the Weber number was elevated to 37.8, the working condition was the critical point for droplet coalescence or separation. It can be found that with an increase in the We number, the time to reach the maximum radial state was advanced, and the amount of deformation increased. It is worth noting that the minimum thickness of the liquid bridge did not appear when the droplet’s radial deformation reached the maximum state (0.31 ms), but when the composite droplet began to shrink under the joint constraint of the interfacial and viscous forces (0.45 ms). Afterward, as the liquid flowed back to the middle, the liquid bridge failed to break and finally coalesced into one. If the We number was further increased, as shown in Figure 4f,g, the composite liquid disk had too large a radial deformation after the collision contact to be retracted into a single droplet. Therefore, the composite droplet split at 0.48 ms and 0.40 ms at the Weber numbers of 40.9 and 54.5, respectively. Moreover, the tiny droplets, after the fragmentation, also retracted into a spherical shape under the action of the surface force. The separation mode during the droplet collision process (Figure 4f,g) can be classified as the “reflexive separation”. The

outcome of the collision (separation or not) is determined by the energy balance between the effective kinetic energy and the surface energy of the temporarily coalesced droplet. The effective kinetic energy consists of the kinetic energies of counteractive flows, excess surface-induced flows, and stretching flows [30]. Ashgriz and Poo [46] deduced that the reflexive separation would occur when the effective kinetic energy is more than 75% of the surface energy of the composite droplets coalesced temporarily.

When the two droplets approach each other, a thin film of air is usually entrapped between them. The drainage process of the air film during the partial engulfment of droplets can be divided into three phases of fast, intermediate, and delayed drainage [26]. In our simulations, although the initial minimum grid size was $2.5\ \mu\text{m}$, the software Fluent employed the dynamic adaption technique (DAT) to automatically refine or coarsen the meshes, where needed, during the simulations. Therefore, the thin film can be well recognized and handled by Fluent. If the full encapsulation was achieved, the simulated small bubble inside the newly formed composite droplet shown in Figure 4c–e was a piece of good evidence.

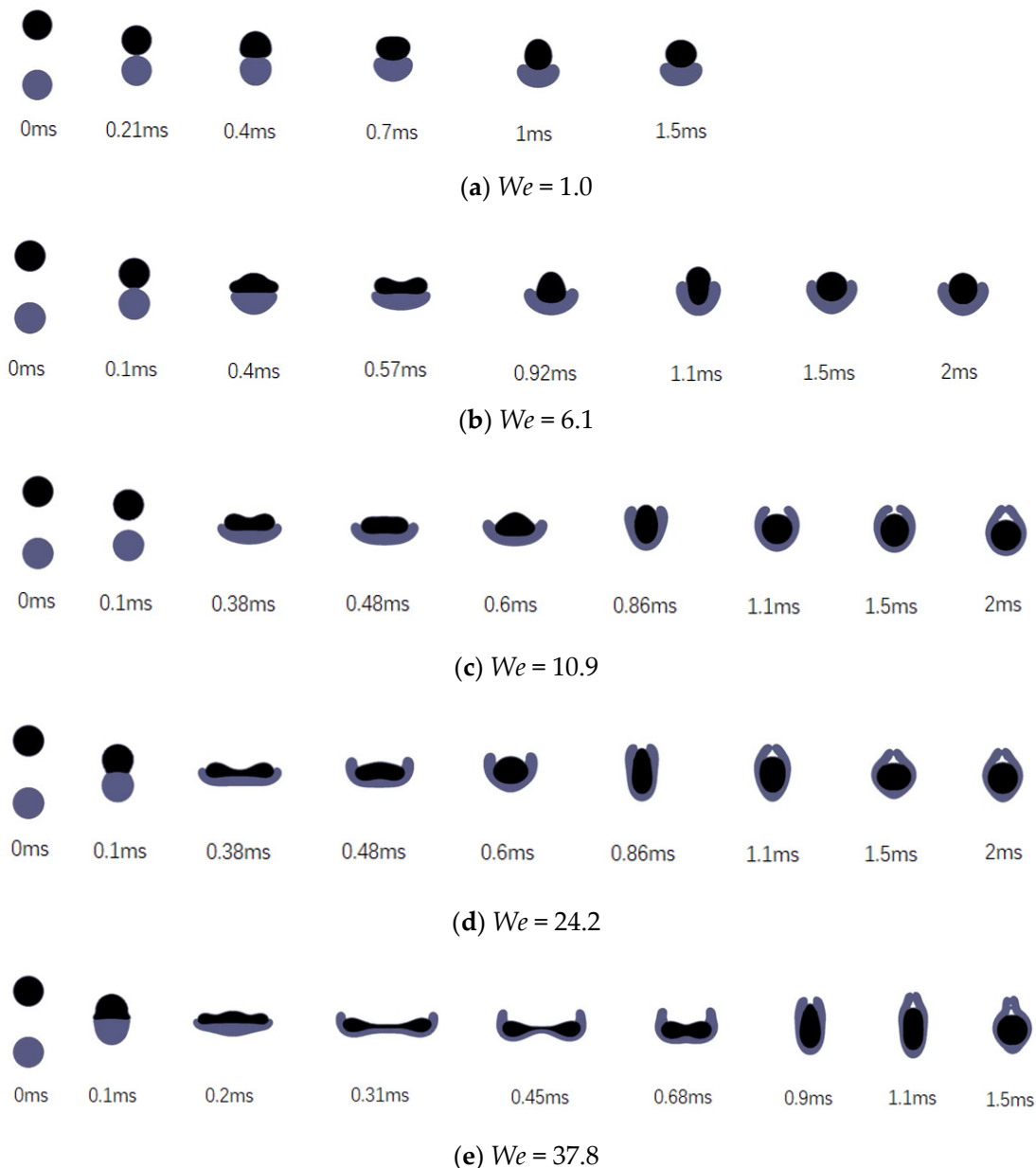


Figure 4. Cont.

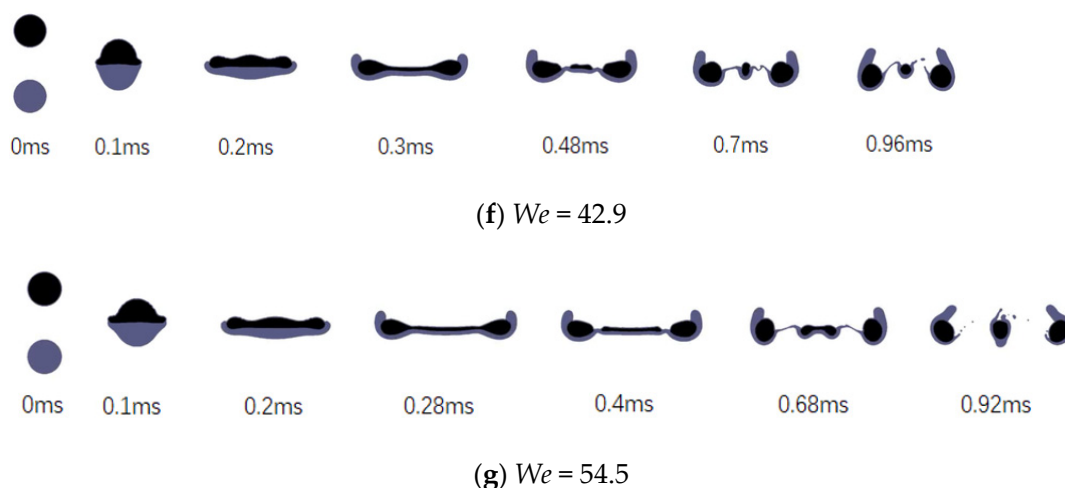


Figure 4. The head-on collision processes between a water droplet and a diesel droplet at different Weber numbers.

Table 2. Physical parameters of the fluids.

Liquid	Density kg m^{-3}	Dynamic Viscosity $\text{mPa}\cdot\text{s}$	Surface Tension mN/m	Interfacial Tension mN/m
Water	998	1.002	72.7	18
Diesel oil	817	3.16	28.85	

The velocity vector graphs shown in Figure 5a–c correspond to the colliding cases with $We = 24.2$, 42.9 , and 54.5 (Figure 4d,f,g), respectively. As shown in Figure 5a, after the contact of the droplets, the velocity distribution decreased with time, which means that the kinetic energy of the colliding droplets was constantly transformed into surface energy or dissipated. As shown in Figure 5b,c, after the formation of the composite liquid disk, the velocity field was relatively uniform before splitting. At the moment of splitting, the flow velocity near the splitting point was close to that of the surrounding air, indicating that the liquid film was splitting in motion. After the split, the flow field had multiple vortices and became more complex.

3.3. Effects of the Liquid Viscosity

3.3.1. Effects of the Viscosity of the Encapsulated Phase

Droplets of the water/glycerol mixture with different viscosities (aqueous phase) colliding with the silicone oil droplets (oil phase) in an air medium were simulated in this study. The droplets' properties are shown in Table 3. The density and surface tension (with air) of the water/glycerol mixture were 1047.9 kg/m^3 and 69.5 mN/m , respectively. The viscosity of the water/glycerol mixture varied from 3.72 to $16.0 \text{ mPa}\cdot\text{s}$. The density, viscosity, and surface tension (with air) of the silicone oil were 944.5 kg/m^3 , $14.28 \text{ mPa}\cdot\text{s}$, and 19.5 mN/m , respectively. Moreover, the interfacial tension between the aqueous phase and the oil phase was 37.7 mN/m .

As shown in Figure 6, the two droplets approached each other with the opposite velocity $U = 1.0 \text{ m/s}$ ($U_r = 2.0 \text{ m/s}$, $We = 11.9$) at the initial moment of collision. Upon contact, two droplets underwent radial expansion, and the kinetic energy was gradually converted into surface energy. The maximum radial deformation of the composite droplet occurred at 0.38 ms . The composite liquid disk then began to shrink under the action of the interfacial and viscous forces, and the disk changed from radial deformation to axial deformation. By observing the results at 0.77 ms and 0.96 ms , it can be seen that when the composite liquid disk changed from axial deformation to radial deformation, the contraction speed of the water phase was faster than that of the oil phase. Consequently,

part of the air will be wrapped in the process of the oil phase wrapping the water phase. Under the condition of $We = 11.9$, by comparing Figure 6a–c, it can be observed that when the viscosity of the water phase increased from 3.72 mPa·s to 16.0 mPa·s, there was little difference in the deformation process of the droplet during the collision. In general, the oil phase tended to gradually wrap the water phase, and full wrapping was complete at about 1.73 ms. By observing the collision results at 0.48 ms and 0.77 ms, it can be seen that with an increase in the viscosity of the aqueous phase (μ_w), the deformation degree of the aqueous phase decreased slightly during the collision process. However, when the viscosity of the aqueous droplet increased to 16.0 mPa·s (shown in Figure 6d), a significant amount of the kinetic energy was consumed by the viscous force, and the residual kinetic energy was not sufficient to overcome the joint action of the viscous force and the surface tension. After several axial and radial deformation transitions, the composite droplet ended up in an incomplete encapsulation state.

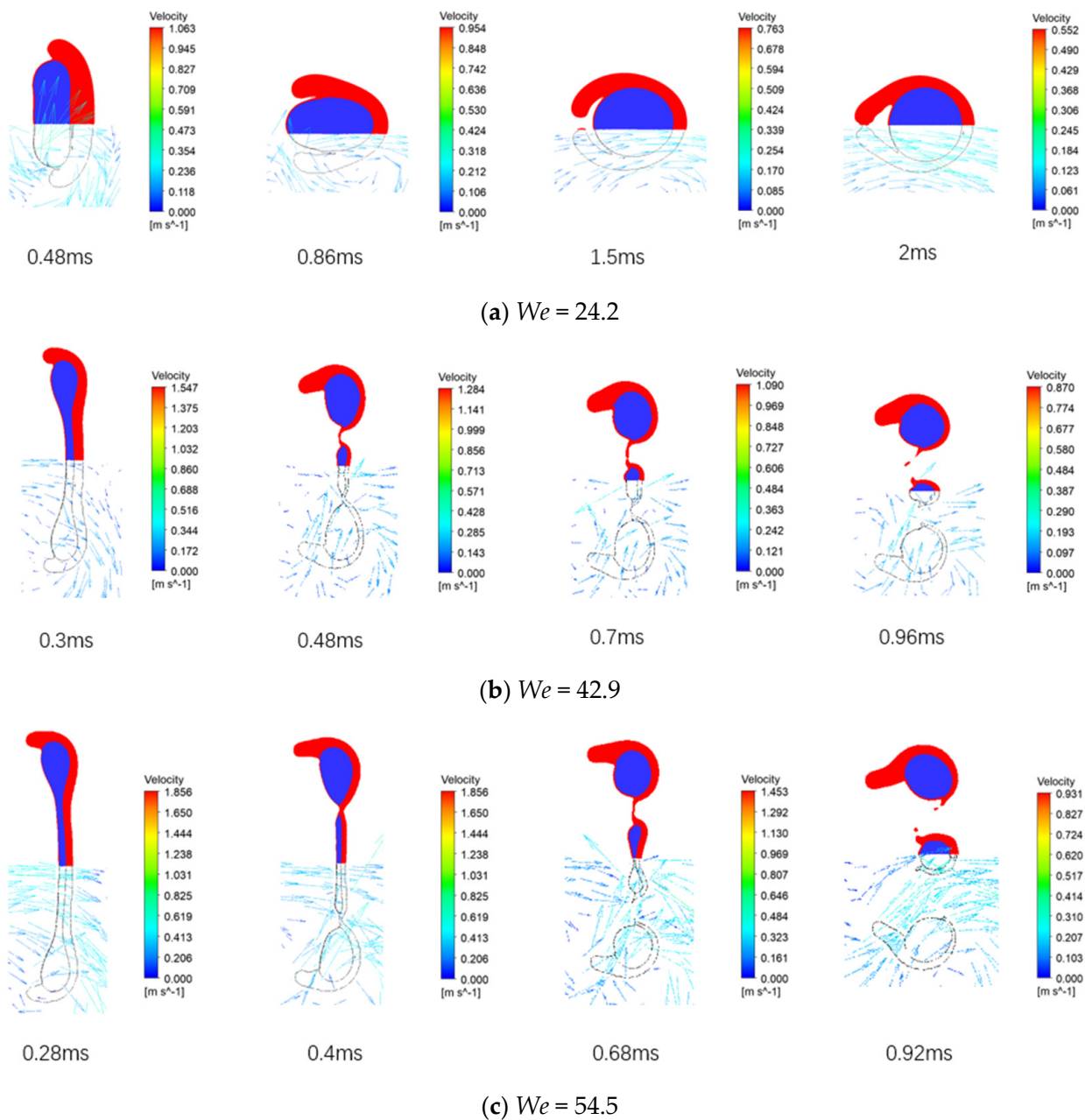
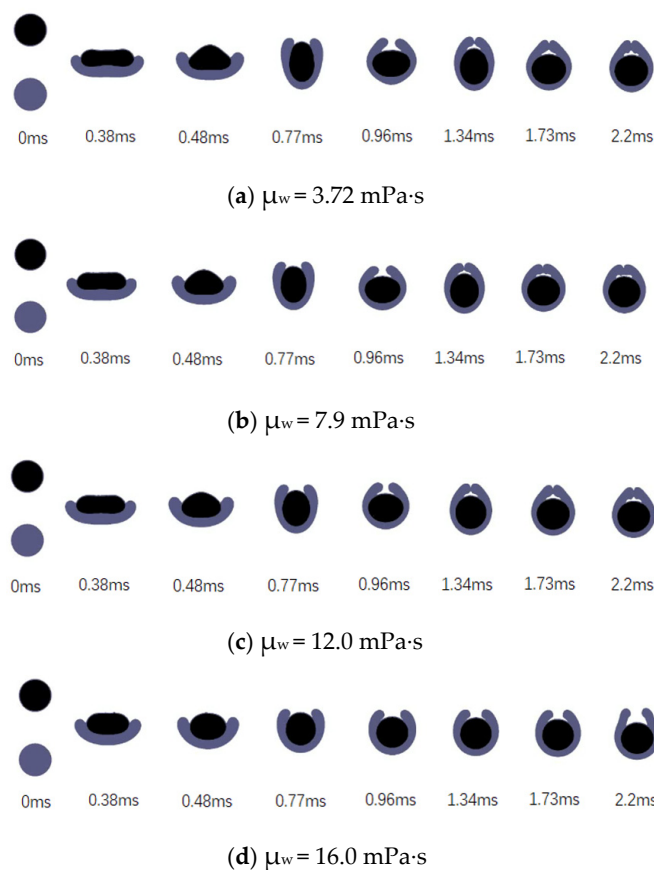


Figure 5. The simulated velocity fields evolve with time.

Table 3. Droplets' physical properties and geometric parameters.

	Droplet 1	Droplet 2
Liquid	Water/glycerol mixture	Silicone oil
Viscosity	3.72–16.0 mPa·s	14.28 mPa·s
Density	1047.9 kg/m ³	944.5 kg/m ³
Surface Tension	69.5 mN/m	19.5 mN/m
D ₀	200.0 μm	200.0 μm
U _r		2.0 m/s

**Figure 6.** Simulated images of the collision process between a water/glycerol droplet and a silicone oil droplet ($We = 11.9$) at different viscosities of the aqueous phase: (a) 3.72 mPa·s; (b) 7.9 mPa·s; (c) 12.0 mPa·s; (d) 16.0 mPa·s.

To find out the influence of the aqueous viscosity on the collision results, the collision process under the condition of $We = 47.7$ ($Ur = 4.0 \text{ m/s}$) was studied further, and the result is shown in Figure 7. By comparing Figures 7a and 6a, it can be seen that the radial expansion increased significantly with an increase in the Weber number. In the process of axial stretching, the greater kinetic energy caused the central liquid bridge to be stretched thinner. At 0.48 ms, the thickness of the liquid bridge reached the minimum. It can be clearly seen that the liquid bridge was about to break at that moment. Eventually, the composite droplet split into two large and one tiny semi-surrounded composite droplets. The small composite droplet and one of the large composite droplets recombined into a fully encapsulated droplet under the action of inertia. As shown in Figure 7b–d, the deformation degree of the newly formed composite droplet decreased with the increase in the viscosity of the aqueous phase, and the fully encapsulation still was realized due to the increase in the kinetic energy. If we compare this with the corresponding Figure 6b–d, it can be concluded that the larger the We number, the greater the degree of deformation.

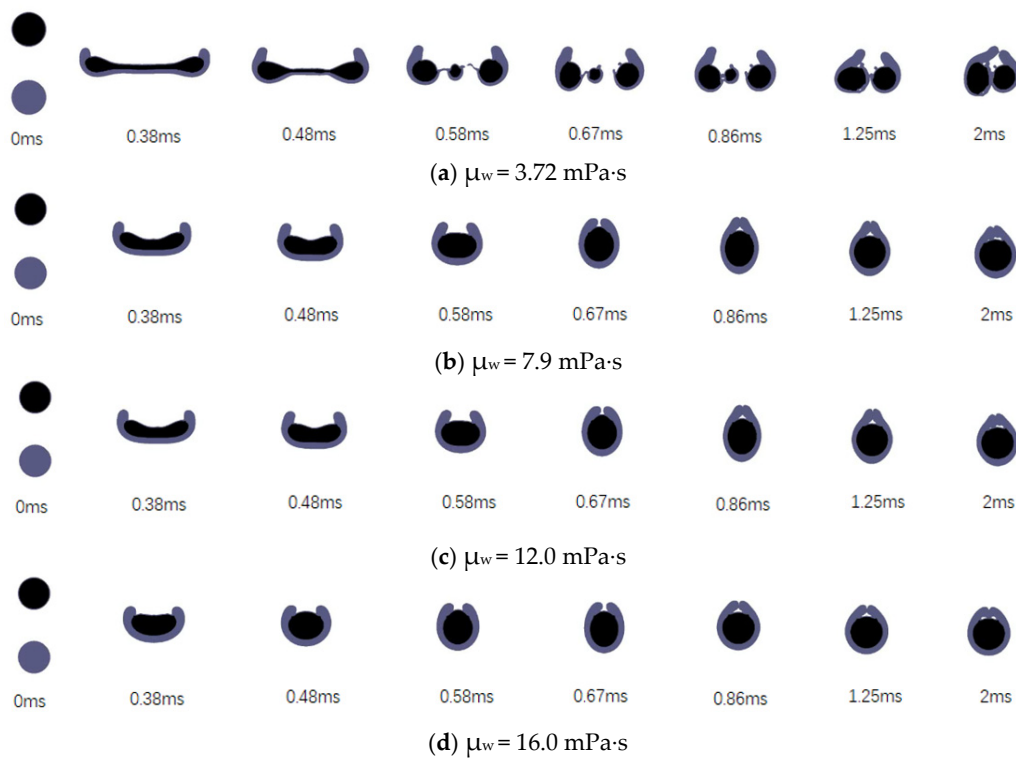


Figure 7. Simulated images of the collision process between a water/glycerol droplet and a silicone oil droplet ($We = 47.7$) at different viscosities of the aqueous phase: (a) 3.72 mPa·s; (b) 7.9 mPa·s; (c) 12.0 mPa·s; (d) 16.0 mPa·s.

3.3.2. Effects of the Viscosity of the Encapsulating Phase

The collision processes between a silicone oil droplet with different viscosities (oil phase) and a water/glycerol droplet (water phase) in an air medium at a constant velocity of $U_0 = 2.0 \text{ m/s}$ ($Ur = 4.0 \text{ m/s}$, $We = 47.7$) are simulated and shown in Figure 8. The droplets' material properties are shown in Table 4.

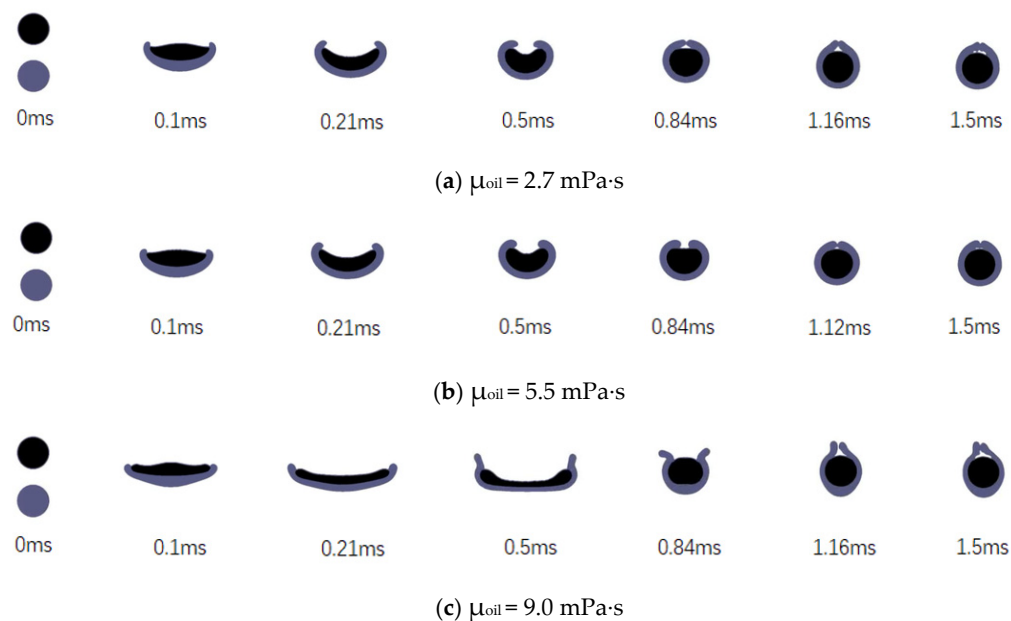


Figure 8. Cont.

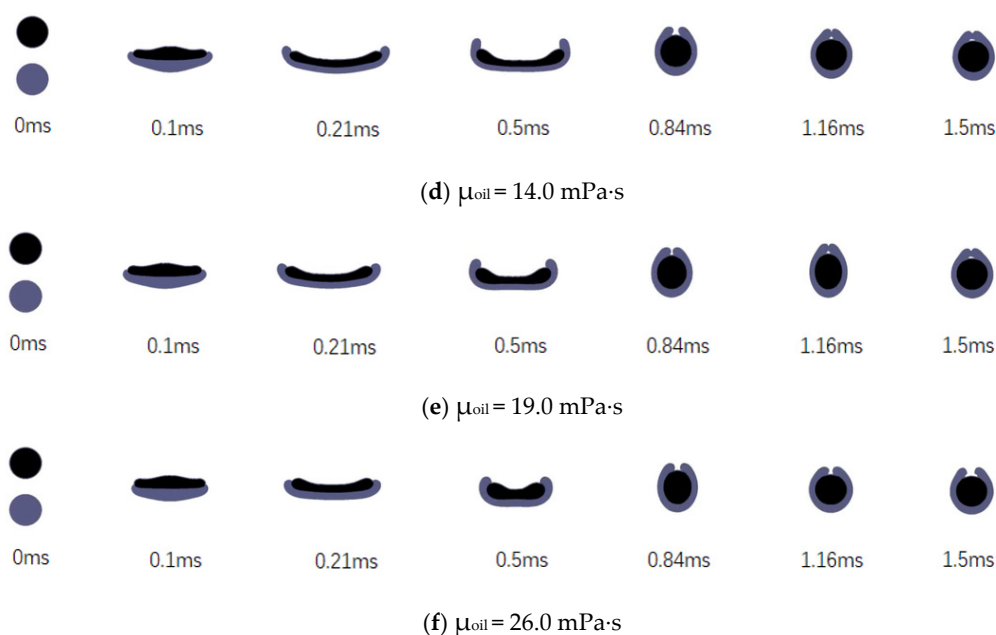


Figure 8. Simulated images of the collision process between a water/glycerol droplet and a silicone oil droplet at different viscosities of the oil phase: (a) 2.7 mPa·s; (b) 5.5 mPa·s; (c) 9.0 mPa·s; (d) 14.0 mPa·s; (e) 19.0 mPa·s; (f) 26.0 mPa·s.

Table 4. Droplets' physical properties and geometric parameters.

	Droplet 1	Droplet 2
Liquid	Water/glycerol mixture	Silicone oils
Viscosity	12.0 mPa·s	2.7–26.0 mPa·s
Density	1098.8 kg/m ³	892.2 kg/m ³
Surface Tension	70.7 mN/m	20.3 mN/m
D ₀	200 μm	200 μm
U _r		4.0 m/s

As shown in Figure 8a, when the viscosity of the oil phase was 2.7 mPa·s, due to the great viscosity difference between the two droplets, the oil phase with less viscosity deformed much faster than the water phase with large viscosity. Therefore, the two droplets quickly formed a half-wrapped state after the collision contact, and formed a fully wrapped state at 0.84 ms. When the viscosity of the oil phase was increased to 5.5 mPa·s (shown in Figure 8b), the viscosity difference between the two droplets was still significant, and the collision process was similar to that in Figure 8a. If we observe the results at 0.84 ms in Figure 8a,b, it can be seen that the former has completed the wrapping while the latter has not. This result confirms the previous conclusion that the higher the viscosity, the slower the deformation process. In Figure 8c, it can be seen that when the viscosity of the oil phase increased to 9.0 mPa·s, the deformation of the liquid disk increased significantly, which is somewhat surprising. If the viscosity of the oil phase rises further, as shown in Figure 8d–f, the deformation of the composite droplet gradually decreases.

Combined with the simulated collision cases of changing the viscosity of the aqueous phase, we believe that the encapsulating droplet (oil phase) and the encapsulated droplet (aqueous phase) play a different role in the encapsulation process. When the viscosity of the oil phase is smaller than that of the aqueous phase, the deformation velocity of the oil phase will be larger than that of the water phase. Before further radial deformation of the aqueous phase, the oil phase has already enveloped the aqueous phase. As shown in Figure 8a,b, the two droplets complete the wrapping with little deformation. With an increase in the oil phase's viscosity (the difference in viscosity between the two droplets decreases), the two

droplets will have a similar deformation velocity after the collision contact. The composite liquid disk deforms significantly during the collision process and eventually reaches a wrapped state (shown in Figure 8c,d). However, with a further increase in the viscosity of the oil phase, the difference in viscosity between the two droplets increases again. At this time, the viscosity of the oil phase is obviously greater than that of the aqueous phase, so the deformation of the oil phase is slower than that of the aqueous phase. Therefore, more kinetic energy is needed to envelop the aqueous drop.

4. Discussions

4.1. Maximum Aspect Ratio

At the end of the first radial deformation after the droplets' collision contact, the composite droplet reaches the maximum expansion in the radial direction. The ratio of the radial diameter of the composite liquid disk to the axial thickness at this moment is defined as the maximum aspect ratio of the composite droplet. The relationships among the maximum aspect ratio, the viscosity of the water or oil phases, and the impact velocity are worth studying.

As shown in Figure 9, the ordinate ζ_{pmax} is the maximum aspect ratio of the composite droplet after the droplet collision, and the abscissa μ_w is the viscosity of the aqueous phase. In all cases, the oil phase is the diesel with a constant viscosity of 14.28 mPa·s. It can be seen from the curve that the maximum aspect ratio ζ_{pmax} of the composite droplet decreases with an increase in the viscosity of the aqueous phase, although the change is not obvious at a low collision velocity. With the same aqueous phase viscosity, the larger the collision velocity, the larger the ζ_{pmax} obtained. Generally speaking, when the viscosity of aqueous droplets is low, the variation in the droplets' velocity has a greater influence on ζ_{pmax} . Otherwise, the influence is smaller. This is because as the viscosity of the aqueous droplets increases, the viscous energy consumed during the radial expansion also increases.

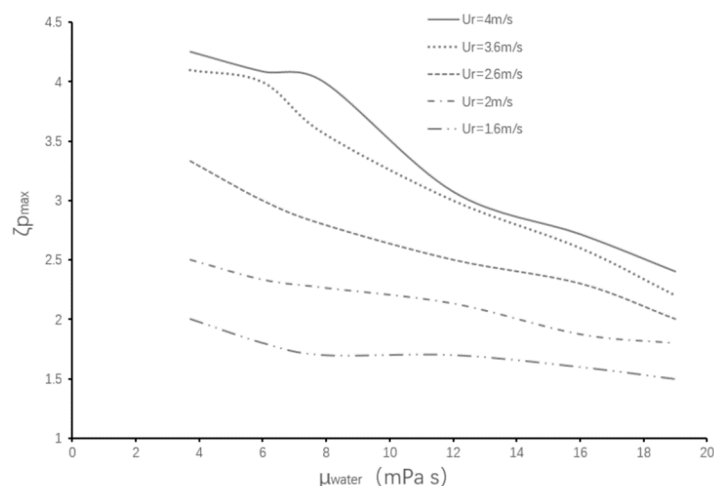


Figure 9. Change in ζ_{pmax} with the aqueous phase's viscosity and the collision velocity.

Similarly, Figure 10 shows the relationships among the maximum aspect ratio of the composite droplet, the viscosity of the oil phase, and the collision velocity. In all cases, the aqueous phase is a glycerol solution with a constant viscosity of 12.0 mPa·s. If the viscosity of the oil phase is kept below 8 mPa·s (i.e., $\mu_{oil} < 8$ mPa·s), the ζ_{pmax} is inversely proportional to the impact velocity under the condition that the viscosity of the oil phase is kept constant. This change relation is not intuitive. It is believed that when the collision velocity is large, the oil phase wraps the water phase rapidly, so the droplets do not undergo great deformation during the collision. However, when the velocity is small, the oil phase will wrap around the water phase relatively slowly, and the droplet has more time to deform. Additionally, if the oil phase viscosity remains smaller than 8.0 mPa·s ($\mu_{oil} < 8.0$ mPa·s) and the collision speed is kept constant, ζ_{pmax} varies proportionally with

the oil phase's viscosity. A reasonable explanation is that when the viscosity of the oil phase is increased to nearly 8.0 mPa·s, the viscosity of the oil phase is close to the viscosity of the water phase. The similar viscosity leads to similar deformation rates, which results in greater deformation. Therefore, when the viscosity of the oil phase increases (varying in the range of less than 8.0 mPa·s), the aspect ratio increases accordingly.

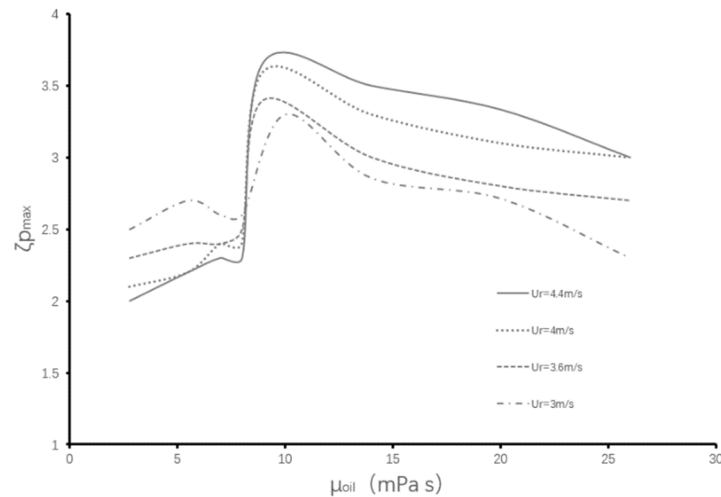


Figure 10. Change in ζ_{pmax} with the oil phase's viscosity and the collision velocity.

When the viscosity of the oil phase increases to more than 8.0 mPa·s ($\mu_{oil} > 8.0$ mPa·s), ζ_{pmax} increases sharply and reaches the peak value if the oil's viscosity varies in the range of 9.0~13.0 mPa·s, and then decreases gradually with an increase in μ_{oil} . This implies that the deformation of the composite liquid disk increases significantly if the oil phase and aqueous phase have a similar viscosity during the collision. The reason is that the deformation of two droplets becomes synchronized due to the similar viscosity, so that the composite droplet can be fully extended.

4.2. Critical Aspect Ratio

In the process of droplet collision, the formed composite liquid disk undergoes the maximum radial deformation and will face two outcomes: coalescence or separation. When the droplet is deformed to the maximum aspect ratio, the only factor that determines its ultimate fate is the aspect ratio of the liquid disk. This is because the disk, at that moment, only has surface energy, so the area and the physical properties of the liquid disk jointly determine the size of the surface energy. The outcome of coalescence or separation is determined by the momentum, the viscous force, and the surface force of the liquid disk at the critical separation time.

To study the effect of the aspect ratio on the evolving results of the composite droplet, we simulated some collision cases with different droplet properties and different collision speeds shown in Table 3. The viscosity of the aqueous droplet (glycerol–water mixture) ranges from 3.72 to 16.0 mPa·s, and the viscosity of the oil droplet (diesel) was constant (14.28 mPa·s). If the collision velocity gradually increased, there was a critical state (Figure 4e is a critical state, for example) when the droplets' collision transitioned from the coalescent state to the splitting state. The maximum aspect ratio of the liquid disk corresponding to the critical state was recorded and called the "critical aspect ratio." As shown in Figure 11, the calculated values of $\zeta_{p,crit}$ are very close to the Rayleigh values of π despite the differences in the viscosity of the aqueous phase. It can be seen that the critical aspect ratio is independent of the aqueous phase's viscosity. Planchette et al. [13] have previously conducted some experimental studies on the critical aspect ratio, and our data are in good agreement with theirs.

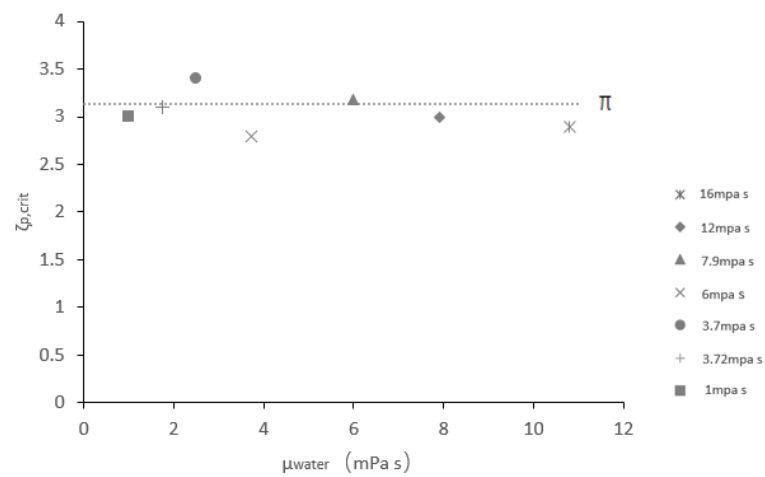


Figure 11. The relationship between $\zeta_{p,crit}$ and the viscosity of the aqueous phase.

4.3. Phase Diagram

Due to the dynamic effect of the outer oil film in the encapsulation process, a bubble will always be formed and wrapped between the aqueous and oil phases [47,48]. In this paper, the collision processes of binary immiscible droplets of different liquids at different collision velocities were simulated. The influences of liquid properties and collision velocities on the collision results were also analyzed. Based on these studies, it was essential to draw the phase diagram of droplet collision regimes characterized by the Weber and Ohnesorge numbers. As shown in Figure 12, if the Weber number is less than 7.0, the outcome of the droplet collision of the immiscible liquids is the coalescence for certain. When the Weber number is greater than 9.0, the fragmentation is the fate of the binary collision of immiscible droplets on the condition that the Ohnesorge number is relatively small. If the Ohnesorge number is increased above a certain value, the encapsulation may be achieved, and then a bubble will be wrapped in the complete package. The size of the wrapped bubble is generally tiny, and its diameter usually ranges from several microns to tens of microns.

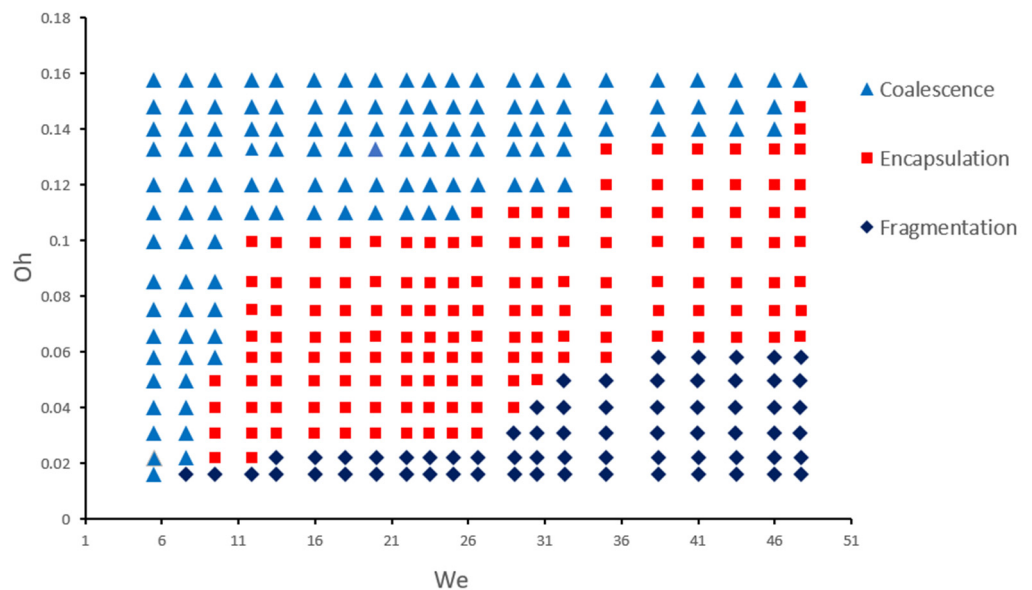


Figure 12. Phase diagram of collision regimes of equal-sized immiscible droplets characterized by the Weber and Ohnesorge numbers.

5. Conclusions

The previous studies on the immiscible droplet collision processes are relatively sparse and are usually restricted to one or two liquid pairs. In this study, the liquid pairs are more abundant. Consequently, the phase diagram of the collision outcome of immiscible droplets depicted in terms of the Weber and Ohnesorge numbers is provided. In future work, a more careful study on the off-center collision of immiscible droplets may be expected. In this study, some conclusions are obtained and listed below.

- (1) Simply increasing the Weber number by increasing the colliding velocity will accelerate the collision process and intensify the degree of deformation.
- (2) Under the condition of low colliding velocities ($We \leq 11.9$), the variation of the viscosity of the encapsulated phase (the aqueous droplet) has little effect on the deformation degree of the droplets during the collision process. Comparatively, the variation of the viscosity of the encapsulating phase (the oil droplet) has a significant effect on the deformation degree of the droplets.
- (3) The critical aspect ratio of the coalescence or fragmentation of the composite droplet is independent of the viscosity of the encapsulated phase (aqueous phase).

Author Contributions: Conceptualization, J.C. (Jiaqing Chang) and Q.S.; methodology, T.S.; validation, R.X. and J.C. (Jinsheng Cui); formal analysis, J.C. (Jinsheng Cui); investigation, R.X. and J.C. (Jiaqing Chang); writing—original draft preparation, R.X.; writing—review and editing, J.C. (Jiaqing Chang); visualization, Q.S.; supervision, T.S. All authors have read and agreed to the published version of the manuscript.

Funding: This research was funded by the Guangzhou Science and Technology Plan Project, grant numbers 202102010461, 202102010408, 202102020320; the Ministry of Science and Technology of the People's Republic of China, grant numbers 2020AAA0104800, 2020AAA0104804; the National Natural Science Foundation of China, grant number 52005116; and the Natural Science Foundation of Guangdong Province, grant number 2020A1515111176.

Conflicts of Interest: The authors declare no conflict of interest. The funders had no role in the design of the study; in the collection, analyses, or interpretation of data; in the writing of the manuscript; or in the decision to publish the results.

References

1. Brazier-Smith, P.R.; Jennings, S.G.; Latham, J. Accelerated rates of rainfall. *Nature* **1971**, *232*, 112–113. [[PubMed](#)]
2. Whelpdale, D.M.; List, R. The coalescence process in raindrop growth. *J. Geophys. Res.* **1971**, *76*, 2836–2856.
3. List, R.; Gillespie, J.R. Evolution of raindrop spectra with collision-induced breakup. *J. Atmos. Sci.* **1976**, *33*, 2007–2013.
4. Bradley, S.G.; Stow, C.D. On the production of satellite droplets during collisions between water drops falling in still air. *J. Atmos. Sci.* **1979**, *36*, 494–500. [[CrossRef](#)]
5. Low, T.B.; List, R. Collision, coalescence, and breakup of raindrops. Part I: Experimentally established coalescence efficiencies and fragment size distributions in breakup. *J. Atmos. Sci.* **1982**, *39*, 1591–1606. [[CrossRef](#)]
6. Tan, Y.C.; Ho, Y.; Lee, A. Droplet coalescence by geometrically mediated flow in microfluidic channels. *Microfluid. Nanofluidics* **2007**, *3*, 495–499.
7. Moreira, A.L.N.; Moita, A.S.; Panão, M.R. Advances and challenges in explaining fuel spray impingement: How much of single droplet impact research is useful? *Prog. Energy Combust. Sci.* **2010**, *36*, 554–580.
8. Sun, K.; Zhang, P.; Law, C.K.; Wang, T. Collision dynamics and internal mixing of droplets of non-Newtonian liquids. *Phys. Rev. Appl.* **2015**, *4*, 054013. [[CrossRef](#)]
9. Doston, S.; Dmitry, E.; Boris, V.B.; Svyatoslav, C.; Stein, T.J.; Iskander, A. Modeling water droplet freezing and collision with a solid surface. *Energies* **2021**, *14*, 1020.
10. Qian, J.; Law, C.K. Regimes of coalescence and separation in droplet collision. *J. Fluid Mech.* **1997**, *331*, 59–80.
11. Brenn, G.; Kalenderski, S.; Ivanov, I. Investigation of the stochastic collisions of drops produced by Rayleigh breakup of two laminar liquid jets. *Phys. Fluids* **1997**, *9*, 349–364.
12. Willis, K.D.; Orme, M. Experiments on the dynamics of droplet collisions in a vacuum. *Exp. Fluids* **2000**, *29*, 347–358.
13. Planchette, C.; Lorceau, E.; Brenn, G. The onset of fragmentation in binary liquid drop collisions. *J. Fluid Mech.* **2012**, *702*, 5–25. [[CrossRef](#)]
14. Demidovich, A.V.; Kralinova, S.S.; Tkachenko, P.P.; Shlegel, N.E.; Volkov, R.S. Interaction of liquid droplets in gas and vapor flows. *Energies* **2019**, *12*, 4256.
15. Huang, K.L.; Pan, K.L. Transitions of bouncing and coalescence in binary droplet collisions. *J. Fluid Mech.* **2021**, *928*, A7.

16. Kropotova, S.; Strizhak, P. Collisions of liquid droplets in a gaseous medium under conditions of intense phase transformations: Review. *Energies* **2021**, *14*, 6150. [[CrossRef](#)]
17. Planchette, C.; Lorenceau, E.; Brenn, G. Liquid encapsulation by binary collisions of immiscible liquid drops. *Colloids Surf. A Physicochem. Eng. Asp.* **2010**, *365*, 89–94.
18. Roisman, I.V.; Planchette, C.; Lorenceau, E.; Brenn, G. Binary collisions of drops of immiscible liquids. *J. Fluid Mech.* **2012**, *690*, 512–535. [[CrossRef](#)]
19. Tang, C.; Zhang, P.; Law, C.K. Bouncing, coalescence, and separation in head-on collision of unequal-size droplets. *Phys. Fluids* **2012**, *24*, 022101.
20. Kavehpour, H.P. Coalescence of drops. *Annu. Rev. Fluid Mech.* **2015**, *47*, 245–268. [[CrossRef](#)]
21. Planchette, C.; Hinterbichler, H.; Liu, M.; Bothe, D.; Brenn, G. Colliding drops as coalescing and fragmenting liquid springs. *J. Fluid Mech.* **2017**, *814*, 277–300. [[CrossRef](#)]
22. Kamp, J.; Villwock, J.; Kraume, M. Drop coalescence in technical liquid/liquid applications: A review on experimental techniques and modeling approaches. *Rev. Chem. Eng.* **2017**, *33*, 1–47.
23. Sommerfeld, M.; Pasternak, L. Advances in modelling of binary droplet collision outcomes in sprays: A review of available knowledge. *Int. J. Multiph. Flow* **2019**, *117*, 182–205.
24. Shlegel, N.; Tkachenko, P.; Strizhak, P. Influence of viscosity, surface and interfacial tensions on the liquid droplet collisions. *Chem. Eng. Sci.* **2020**, *220*, 115639.
25. Focke, C.; Kuschel, M.; Sommerfeld, M.; Bothe, D. Collision between high and low viscosity droplets: Direct numerical simulations and experiments. *Int. J. Multiph. Flow* **2013**, *56*, 81–92.
26. Choi, S.B.; Lee, J.S. Film drainage mechanism between two immiscible droplets. *Microfluid. Nanofluidics* **2014**, *17*, 675–681.
27. Zhang, J.T.; Liu, H.R.; Ding, H. Head-on collision of two immiscible droplets of different components. *Phys. Fluids* **2020**, *32*, 082106. [[CrossRef](#)]
28. Leclaire, S.; Reggio, M.; Trépanier, J.Y. Progress and investigation on lattice Boltzmann modeling of multiple immiscible fluids or components with variable density and viscosity ratios. *J. Comput. Phys.* **2013**, *246*, 318–342.
29. Sussman, M.; Smereka, P.; Osher, S. A level set approach for computing solutions to incompressible two-phase flow. *J. Comput. Phys.* **1994**, *114*, 146–159. [[CrossRef](#)]
30. Ko, G.H.; Ryou, H.S. Modeling of droplet collision-induced breakup process. *Int. J. Multiph. Flow* **2005**, *31*, 723–738.
31. Wörner, M. Numerical modeling of multiphase flows in microfluidics and micro process engineering: A review of methods and applications. *Microfluid. Nanofluid.* **2012**, *12*, 841–886. [[CrossRef](#)]
32. Mohammadi, M.; Shahhosseini, S.; Bayat, M. Direct numerical simulation of water droplet coalescence in the oil. *Int. J. Heat Fluid Flow* **2012**, *36*, 58–71. [[CrossRef](#)]
33. Yuan, S.; Dabirian, R.; Shoham, O.; Mohan, R.S. Numerical simulation of liquid droplet coalescence and breakup. *J. Energy Resour. Technol.* **2020**, *142*, 102101.
34. Inamuro, T.; Tajima, S.; Ogino, F. Lattice Boltzmann simulation of droplet collision dynamics. *Int. J. Heat Mass Transf.* **2004**, *47*, 4649–4657.
35. Lycett-Brown, D.; Luo, K.H.; Liu, R.; Lv, P. Binary droplet collision simulations by a multiphase cascaded lattice Boltzmann method. *Phys. Fluids* **2014**, *26*, 023303. [[CrossRef](#)]
36. Liang, H.; Shi, B.; Chai, Z. Lattice Boltzmann modeling of three-phase incompressible flows. *Phys. Rev. E* **2016**, *93*, 013308.
37. Ebadi, A.; Hosseinalipour, S.M. The collision of immiscible droplets in three-phase liquid systems: A numerical study using phase-field lattice Boltzmann method. *Chem. Eng. Res. Des.* **2022**, *178*, 289–314. [[CrossRef](#)]
38. Morris, J.P.; Fox, P.J.; Zhu, Y. Modeling low Reynolds number incompressible flows using SPH. *J. Comput. Phys.* **1997**, *136*, 214–226.
39. Hirschler, M.; Oger, G.; Nieken, U.; Touzé, D.L. Modeling of droplet collisions using smoothed particle hydrodynamics. *Int. J. Multiph. Flow* **2017**, *95*, 175–187. [[CrossRef](#)]
40. Nishio, Y.; Komori, K.; Izawa, S.; Fukunishi, Y. Simulation of collisions of two droplets containing two different liquids using incompressible smoothed particle hydrodynamics method. *Theor. Comput. Fluid Dyn.* **2020**, *34*, 105–117.
41. Gao, T.C.; Chen, R.H.; Pu, J.Y.; Lin, T.H. Collision between an ethanol drop and a water drop. *Exp. Fluids* **2005**, *38*, 731–738. [[CrossRef](#)]
42. Chen, R.H.; Chen, C.T. Collision between immiscible drops with large surface tension difference: Diesel oil and water. *Exp. Fluids* **2006**, *41*, 453–461.
43. Chen, R.H. Diesel–diesel and diesel–ethanol drop collisions. *Appl. Therm. Eng.* **2007**, *27*, 604–610. [[CrossRef](#)]
44. Zhang, M.Y.; Zhao, H.; Xu, J.H.; Luo, G.S. Controlled coalescence of two immiscible droplets for Janus emulsions in a microfluidic device. *RSC Adv.* **2015**, *5*, 32768–32774.
45. Piskunov, M.V.; Shlegel, N.E.; Strizhak, P.A.; Volkov, R.S. Experimental research into collisions of homogeneous and multi-component liquid droplets. *Chem. Eng. Res. Des.* **2019**, *150*, 84–98. [[CrossRef](#)]
46. Ashgriz, N.; Poo, J.Y. Coalescence and separation in binary collisions of liquid drops. *J. Fluid Mech.* **1990**, *221*, 183–204. [[CrossRef](#)]

-
47. Freitas, L.G.; Pereira, L.A.A.; Silva, A.L.F.L. Comparison among drag coefficient models of single bubbles under high and low Morton number regimes. *Chem. Eng. Sci.* **2021**, *236*, 116473. [[CrossRef](#)]
 48. Rivière, A.; Ruth, D.J.; Mostert, W.; Deike, L.; Perrard, S. Caillary driven fragmentation of large gas bubbles in turbulence. *Phys. Rev. Fluids* **2022**, *7*, 083602.